Theor Chem Acc (2011) 129:247–255
DOI 10.1007/s00214-011-0928-6

REGULAR ARTICLE

The influence of thienyl-*S*,*S*-dioxidation on the photoluminescence and charge transport properties of dithienothiophenes: a theoretical study

Yun Geng · Haibin Li · Shuixing Wu · Yuai Duan · Zhongmin Su · Yi Liao

Received: 16 February 2011 / Accepted: 16 March 2011 / Published online: 31 March 2011

Abstract Fused thiophenes have been an important class of materials due to their intriguing organic optoelectronic application. Here, comparative theoretical investigation on the fluorescence and charge transport properties of dithienothiophene compounds (**1** and **2**) and their dioxide derivatives (**3** and **4**) was carried out to shed light on the role of the thienyl-*S*,*S*-dioxide unit. The lower HOMO, LUMO energy levels, and red-shift spectra (absorption and emission) of **3** and **4** compared with **1** and **2** were attributed to the electron-withdrawing nature of the thienyl-*S*,*S*-dioxide unit. The phenomenon that fluorescence quantum yield of **4** was significantly increased through thienyl-*S*,*S*-dioxidation, compared with those of **1** and **2**, was analyzed by the evaluations of the radiative decay rates and the radiationless decay rates in theory at the single molecule level and the simulation of absorption spectrum of dimer of **1**. For **1**, a much higher hole mobility (0.12 cm^2/V.s) calculated by carrier hopping model than the experimental value $\sim 10^{-4}$ cm^2/V.s was also further elucidated by molecular dynamics simulation. Furthermore, a preliminary investigation of the transport property of **3** was performed by combining the molecular dynamics simulation with dispersion-corrected B3LYP functional to provide insight into the effect of thienyl-*S*,*S*-dioxidation on the charge transport.

Keywords Dithienothiophene · Thienyl-*S*,*S*-dioxide · Optoelectronic property · Density functional theory

1 Introduction

Thiophene-based oligomers hold considerable potential in applications as diverse as organic light-emitting diodes (OLED) [1, 2], organic field effect transistors (OFET) [3–5], and organic photovoltaic cells (OPV) [6]. Large π-conjugation and outstanding chemical and physical properties of oligothiophenes make them attract much more interest of research from both experimentalists and theoreticians [7, 8]. In general, unsubstituted oligothiophenes display very low photoluminescence quantum yield in the solid state [9, 10], and they only exhibit p-type hole transport properties, restricting their multifunctional application. To this end, Barbarella et al. [1, 11–15] have devoted much effort to the chemical modification of thienyl sulfur into the thienyl-*S*,*S*-dioxidation for the purpose of improving the solid-state photoluminescence efficiencies and increasing electron affinities and thus their air stability. Thereby, they synthesized many dioxidations of oligothiophenes, including α,ω-bissilylated oligothiophenes *S*,*S*-dioxides, 3,5-dimethyldithieno[3,2-b;2′,3′-*d*]-thiophene-4,4-dioxides, and so on. Recently, many new thiophene *S*,*S*-dioxides have been reported with excellent optoelectronic properties [15–18]. In addition, Tanaka et al. [19] reported early in 1989 the first theoretical investigation on the band gap and stability of *S*,*S*-dioxide derivatives compared to oligothiophenes using the semi-empirical tight-binding SCF-CO (self-consistent

Electronic supplementary material The online version of this article (doi:10.1007/s00214-011-0928-6) contains supplementary material, which is available to authorized users.

Y. Geng · H. Li · S. Wu · Y. Duan · Z. Su (✉)
Institute of Functional Material Chemistry,
Faculty of Chemistry, Northeast Normal University,
Changchun 130024, People's Republic of China
e-mail: zmsu@nenu.edu.cn

Y. Liao (✉)
College of Chemistry, Capital Normal University,
Beijing 100048, People's Republic of China
e-mail: liaoy271@nenu.edu.cn

field-crystal orbital) method, which has been used to calculate the band structures and electronic properties of one-dimensional polymers. Subsequently, some discussions on the photoluminescence properties were presented [15]. However, the comprehensive insight into the influence of thienyl-*S*,*S*-dioxidation on the photoluminescence and transport properties of oligothiophenes in theory is sparse.

Recently, Afonina et al. [20] have synthesized three new diindenodithienothiophene-based materials **1**, **2,** and **4** (see Fig. 1). Compound **4**, a *S*,*S*-dioxide of fused thiophene **2**, exhibits some interesting phenomena, such as the lower energy gap between HOMO and LUMO and the higher photoluminescence quantum yield when compared to the parent-fused thiophene **2** (or **1**). To our surprise, compound **1,** which has the much ordered π–π stacking, exhibits an abnormally low hole mobility (only 10^{-4} $cm^2/V{\cdot}s$). This low mobility is in marked contradiction with our conventional wisdoms, namely the organic materials with ordered π–π stackings should have high mobilities, and OFETs prepared with fused thiophenes present high hole mobilities generally [21–25]. As a result, it is of extreme importance to understand and rationalize the intrinsic mechanism behind these abnormities, paving the way to design and develop high-efficient and multifunctional materials.

In the present work, our initial interest was sparked by the significant increase in the photoluminescence quantum yield for **4** upon dioxdation and the anomalously low mobility of **1**. Thus, comprehensive quantum chemistry calculations were carried out in an attempt to demonstrate the influence of thienyl-*S*,*S*-dioxide on the photoluminescence and charge transport properties. The frontier molecular orbitals, electronic spectra, the radiative decay rates, the nonadiabatic radiationless decay rates, and simulated absorption spectrum of a dimer of **1** were probed in detail to provide insight into the much lower fluorescence quantum yield of **1** compared with **4**. Then, for the hole transport properties, we also analyzed the reorganization energies and transfer integrals. In particular, the thermal fluctuation of the transfer integrals along major carrier hopping direction was also investigated to give a further understanding of the discrepancy between the calculated hole mobility and experimental datum of **1**. Moreover, the packing of some dimers of the theoretical simplified model **3** obtained from molecular dynamics (MD) simulation was determined and re-optimized by employing dispersion-corrected B3LYP functional to give a preliminary description of transport property of the *S*,*S*-dioxidation of fused thiophene, which has not been discussed in theory so far. We hope that our investigation on the dioxidation of dithienothiophenes can provide guideline for the design of new materials.

2 Computational and theoretical methodology

Density functional theory (DFT) calculations have been proved to give a good description of geometries and molecular orbital distributions for thiophene compounds [26]. Here, three functionals, B3LYP, B3PW91, and PBE0, were employed to optimize the geometry of **1** with the same basis set 6-31G(d,p) to determine the optimal functional. The optimized geometries of **1** obtained from the three functionals were compared with experimental values, which are depicted in Fig. S1 in the supplementary material. The results indicate that the B3PW91 functional gives the smallest deviations of the bond lengths among these functionals. In other words, B3PW91 functional was the most appropriate functional among them to describe the geometries of the compounds investigated here. Thereby, the ground-state geometries of all compounds were

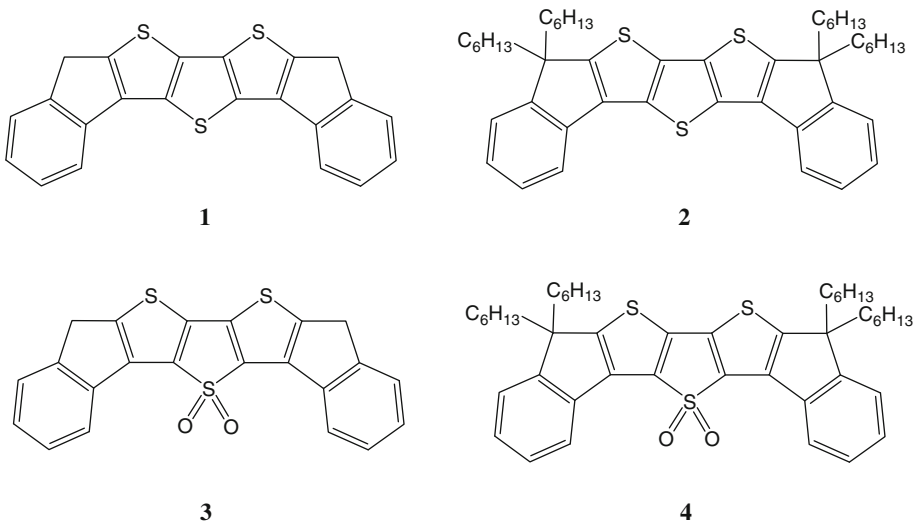

Fig. 1 Molecular models investigated here in this work

optimized at B3PW91/6-31G(d,p) level, and the time-dependent density functional theory (TDDFT/B3PW91) was employed to optimize the lowest singlet excited-state geometries and to investigate their absorption and emission spectra. The effect of the solvent (chloroform) within polarizable continuum model (PCM) [27] was taken into account during the calculation of excitation energies. All the calculations were performed with the Gaussian 09 program package [28].

The hole transport properties of **1** and theoretical simplified model **3** were estimated in terms of the carrier hopping model, which has been generally considered to be appropriate to describe the carrier transport of organic semiconductors at room temperature [29]. In hopping regime, the hopping rate can be described by Marcus theory [30, 31]:

$$k = V^2 \sqrt{\frac{\pi}{\hbar^2 k_B T \lambda}} \exp\left(-\frac{\lambda}{4 k_B T}\right) \tag{1}$$

where V and λ represent the transfer integral (also referred to the electronic coupling) and the reorganization energy, respectively. $\hbar$ is the reduced Planck constant, k_B is the Boltzmann constant, and T is the temperature. Therefore, the transfer integral and reorganization energy are two key parameters determining carrier hopping rate. And, we employed the site-energy corrected method [32] to evaluate the transfer integral values for all hopping pathways selected from crystal structure of **1** and optimized dimer of **3**. This method is selected to calculate the effective transfer integral and effective site energies from the spatial overlap integral S_{12}, transfer integral V_{12}, and site energies $\varepsilon_{1(2)}$,

$$V_{12}^{eff} = \frac{V_{12} - \frac{1}{2}(\varepsilon_1 + \varepsilon_2) S_{12}}{1 - S_{12}^2} \tag{2}$$

$$\varepsilon_{1(2)}^{eff} = \frac{1}{2} \frac{(\varepsilon_1 + \varepsilon_2) - 2V_{12}S_{12} \pm (\varepsilon_1 + \varepsilon_2)\sqrt{1 - S_{12}^2}}{1 - S_{12}^2}. \tag{3}$$

Assuming that H is the Hamiltonian of the dimer system, and ψ_1 and ψ_2 are the highest occupied molecular orbitals (HOMOs) or the lowest unoccupied molecular orbitals (LUMOs) of two monomers. S_{12}, V_{12}, and $\varepsilon_{1(2)}$ needed for the calculation of transfer integral can be obtained from $S_{12} = \langle \psi_1 | \psi_2 \rangle$, $\varepsilon_{1(2)} = \langle \psi_{1(2)} | H | \psi_{1(2)} \rangle$ and $V_{12} = \langle \psi_1 | H | \psi_2 \rangle$. All calculations were performed at PW91PW91/6-31G(d,p) level, which has been demonstrated to give better results [33, 34]. In general, the reorganization energy is cast into contributions from intramolecular vibrations and surrounding medium, namely internal reorganization energy and the external reorganization energy, respectively. Here, the intramolecular reorganization energies of all compounds were evaluated from adiabatic potential-energy surfaces (provided in supplementary material) at B3PW91/6-31G(d,p) level, while the external reorganization energies were ignored due to its extremely small contributions to total reorganization energies of the planar conjugation molecules [35, 36].

At a fixed temperature (T), the carrier mobility is calculated with the Einstein relation:

$$\mu = \frac{e}{k_B T} D \tag{4}$$

where e is the electronic charge, D is the diffusion coefficient, which is related to the charge-transfer rate k, and it can be approximately evaluated as $D = (1/2d) \cdot \Sigma r_i^2 k_i P_i$. i represents a specific hopping pathway with r_i being the electron hopping distance; d is spatial dimension while $P_i = k_i / \Sigma k_i$ is the relative probability for electron hopping to the ith neighbor. The calculations of all parameters aforementioned were performed on the basis of the three-dimensional crystal structure of **1** and optimized dimer of **3** selected from MD simulation results (vide infra).

To give a preliminary estimate of carrier transport property of **3** with thienyl-*S*,*S*-dioxide unit, an amorphous film of **3** including 30 molecules was constructed and optimized in Materials Studio package with COMPASS force field [37], which has been demonstrated to reproduce the experimental crystal structures of oligoacenes extremely well [38, 39]. Then, this film was further optimized using MD simulation to obtain molecular packing for some dimers. Among them, the stablest dimer was singled out and optimized by means of dispersion-corrected method (B3LYP-D) with the default parameters found in the ORCA package [40]. The basis set is cc-pVDZ, as reference [41] proposed. On the basis of the optimized dimer, the transfer integral and carrier hopping rate were also evaluated. Furthermore, to give a further study on the discrepancy between the calculated hole mobility and experimental value of **1**, the modulation of the transfer integral by thermal motions along the major hopping direction was investigated through MD simulation. The procedure was descried in detail in reference [42].

3 Results and discussions

3.1 Geometric and electronic structures

All the molecular structures were fully optimized without symmetry constraints at the B3PW91/6-31G(d,p) level, as mentioned above. The nature of the stationary points was confirmed by means of vibrational frequency analysis at the same level.

The geometry of **1** obtained from calculation is in good agreement with the experimental structures, as shown in

the Fig. S1. The structural deviations fall well within 0.01 Å, giving the confidence in the accuracy of the calculated geometries. The influences of the alkylation and thienyl-*S*,*S*-dioxide unit on the geometry structure of **1** were investigated, and the bond lengths of the four compounds are collected in Table S1. The results indicate that the alkylation has a negligible effect on the structures, and the thienyl-*S*,*S*-dioxide units bring into large changes of bond lengths of central thiophenes, especially for much increase in bond length of S1-C2.

The HOMOs and LUMOs of all compounds are depicted in Fig. 2. It is found that there is no significant difference in the energy level and orbital distribution of the simplified model **3** in comparison with its hexyl side-chain substituent **4**. The simplification is justified because alkyl substituents are not conjugated with the aromatic rings, and thus, they are not supposed to exert any remarkable influence on the electronic structure of the aromatic system. Compared with **1** and **2**, the thienyl-*S*,*S*-dioxide unit in **3** and **4** lowers obviously the frontier molecular orbital energies, especially for the LUMOs; the dioxide unit also has an influence on the localization of the LUMOs within the central three thiophenes. To understand the role of thienyl-*S*,*S*-dioxide unit, molecular orbital correlation diagrams obtained from charge decomposition analysis [43] were depicted in Fig. S2. It shows that the LUMO of **1** is mainly contributed from the α-LUMO (91.0%) and β-LUMO + 2 (95.1%) of fragment **1′** (the whole molecule except for sulfur) and the α-LUMO (4.2%) of fragment sulfur with antibonding character of carbon–sulfur bonds. Thus, the energy level of LUMO of **1** should be higher than that of **1′** in terms of orbital interaction theory. While for **3**, the LUMO mainly comes from the contributions of the α-LUMO (77.7%) and β-LUMO + 2 (58.7%) of fragment **1′** and the α-LUMO + 1 (9.1%) and β-LUMO + 3 (8.5%) of fragment SO_2, having bonding orbital character of carbon–sulfur bonds, the LUMO energy levels of **3** and **4** are lowered. These characters are in good agreement with the electron density distribution of LUMOs shown in Fig. 2. Simultaneously, the lower LUMO levels of **3** and **4** imply that their electron affinities should be in favor of their ambipolar charge transport characters.

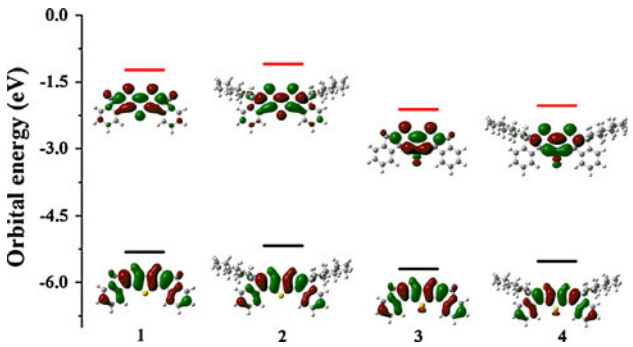

Fig. 2 Illustration of the frontier molecular orbitals for all compounds at B3PW91/6-31G(d,p) level

From the standpoint of carrier transport, the more delocalization of the frontier molecular orbital is, the more favorable carrier transport is [44]. The similar delocalization degrees of the HOMOs for **1** and **3** suggests that these two compounds may possess similar hole transport performances.

3.2 Electronic spectra

Currently, TDDFT approach has been considered as a cost-effective method to provide the satisfactory estimate of electronic transition energies of π-conjugated molecules [45]. Our group has developed the machine learning methods to further reduce the errors of the TDDFT method [46, 47]. Herein, the electronic transition properties of all compounds evaluated at TD-PCM-B3PW91/6-31G(d,p) level are summarized in Table 1. Figure 3 compares the experimental and theoretical absorption spectra of compound **1** and **4**. The agreement between the measured and simulated spectra is fair well, in both band positions and overall spectral shape.

According to Table 1, the vertical excitations of the simplified model **3** are similar to those of **4**, suggesting that the introduction of alkyl chains has little influence on the absorption properties of π-conjugated systems and further confirming that the model simplification for **3** is reasonable. In addition, the essentially same absorptions for **1** and **2** indicate that our strategy, replacing the long alkyl chains with hydrogen atoms, is viable, while more complicated transitions in **1** and **2** relative to their *S*,*S*-dioxide substituents **3** and **4** would be a manifestation of a more localized excited state in the latter, resulting from their comparatively localized LUMOs upon the introduction of electron-withdrawing substituents. As seen from Fig. 3, there are two absorption peaks of **1**, of which the higher-energy absorption peak recorded at 284 nm is considered as the maximum absorption in experiment. To visualize the electron transition process, the corresponding changes of electron density distribution of major absorption peaks were calculated and are displayed in Fig. 4. Combining Table 1 and Fig. 4, we can find that the low-energy absorption peak of **1** comes from HOMO to LUMO mainly assigned to π–π* transition, while the high-energy absorption peak of **1** assigned to $S_0 \rightarrow S_8$ is mainly ascribed to electron transfer from central thiophenes to cyclopentadienes and benzene rings. While for **4**, only one absorption peak is predicted around 421 nm, being in good agreement with the experimental value (419 nm). We associate the absorption peak with the transition from HOMO to LUMO, which are delocalized π- and somewhat localized π*-orbitals, respectively, showing a obvious

Table 1 The calculated absorption energies (nm), oscillator strengths (*f*), major contributions, together with the experimental values of all compounds

Compounds	State	$\lambda_{cal.}$	*f*	Major contribution	$\lambda_{exp.}$[a]
1	S_1	330	0.42	HOMO → LUMO (97%)	352
	S_3	292	0.19	HOMO-1 → LUMO (23%)	
				HOMO → LUMO + 1 (69%)	
	S_4	285	0.21	HOMO → LUMO + 2 (91%)	
	S_7	269	0.2	HOMO-1 → LUMO + 1 (35%)	284
				HOMO → LUMO + 4 (55%)	
	S_8	267	0.4	HOMO-2 → LUMO (23%)	284
				HOMO-1 → LUMO + 1 (45%)	
				HOMO → LUMO + 4 (22%)	
2	S_1	333	0.55	HOMO → LUMO (97%)	340
	S_3	295	0.18	HOMO-1 → LUMO (50%)	
				HOMO → LUMO + 1 (42%)	
	S_4	291	0.27	HOMO → LUMO + 2 (94%)	
	S_8	268	0.44	HOMO-2 → LUMO (12%)	273
				HOMO-1 → LUMO + 1 (78%)	
3	S_1	414	0.47	HOMO → LUMO (98%)	
4	S_1	421	0.58	HOMO → LUMO (98%)	419

[a] Data from reference [20]

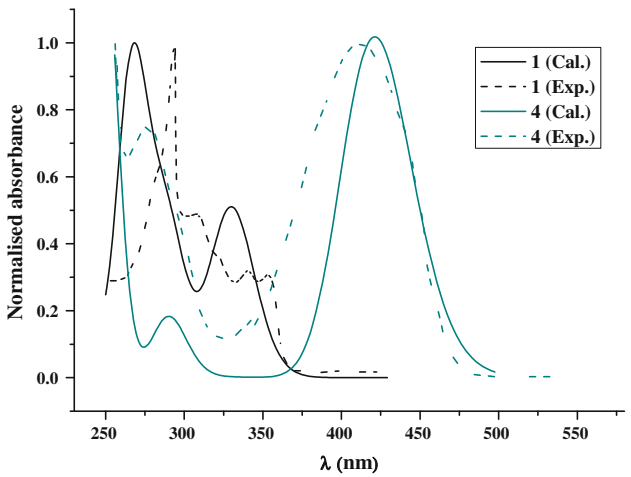

Fig. 3 Normalized spectra of **1** and **4** calculated (*solid line*) at their optimized ground-state geometries by TDDFT in chloroform solvent with their experimental absorption spectra (*dash line*)

electron transfer from two ends to central thiophenes and thienyl-*S*,*S*-dioxide unit. Therefore, a red-shift of about 135 nm in the maximum absorption is evaluated from **1** to **4** due to the incorporation of electron-withdrawing thienyl-*S*,*S*-dioxide moiety, which induces large decrease in the LUMO energy level as mentioned above.

3.3 Fluorescence quantum yield

The geometry optimization of the first singlet excited-state geometries of all compounds and the emissions were performed at TD-B3PW91/6-31G(d,p) level to set the stage for the discussion on the difference in fluorescent quantum yields due to dioxidation. The emission energies, oscillator strengths, main configurations together with the available experimental emission maxima are collected in Table 2. It shows that the calculated values are in very good agreement with experimental ones and that the major contribution of $S_1 \rightarrow S_0$ for each compound arises from the electronic transition from LUMO to HOMO. Moreover, the emission energy of **4** is much less than those of **1** and **2**, which is consistent with the decrease of LUMO in **4**. Thus, we can reasonably infer that the fluorescent quantum yield of **4** should be lower based on energy-gap law. However, it was reported that the photoluminescence quantum yield of **4** is much larger than that of **1** upon dioxidation.

Here, we tried to find the structural and electronic factor, which has an important relationship with photoluminescence quantum yield, by means of detailed theoretical calculations and analysis. As we know, the fluorescence quantum yield can be expressed as $\eta = k_r/(k_r + k_{nr})$, where k_r is the radiative decay rate, k_{nr} consists of the nonradiative decay to ground state, including the internal conversion and the intersystem crossing process. So it can follow from this expression that large k_r and small k_{nr} would lead to large fluorescence quantum yield. In what follows, we first calculated the k_r through the Einstein spontaneous emission relationship, $k_r = f \cdot E_{if}^2/1.499$, wherein *f* is the oscillator strength and E_{if} is the excitation energy in cm^{-1}. Referring to Table 2, the radiative decay rates of **1** and **4** were calculated to be 2.41×10^8 s^{-1} and 1.20×10^8 s^{-1}, respectively. As for **4**, a natural radiative lifetime of $9.8 \sim 12$ ns has been reported in chloroform solution, that is, the radiative decay rate of **4** is $0.8 \sim 1.02 \times 10^8$ s^{-1}. Thus, the theoretical evaluations of radiative decay rates using Einstein spontaneous emission relationship are accurate and reliable for our systems. Apparently, k_r is not the crucial factor affecting quantum yield. Next, we thus turn our attention to the radiationless decay rate.

As far as k_{nr} was concerned, we first qualitatively discussed geometrical relaxations from the first singlet excited state to ground state, i.e., the internal conversion process. It is established that Huang–Rhys factor characterizing electron-vibration coupling strength is an important physical quantity identifying radiationless decay process [23, 48, 49]. Its formula is $S_j = (\omega_j \Delta Q_j^2)/2\hbar$, where ω_j represents vibration frequency for the *j*th mode and ΔQ_j is the normal-mode displacement. The geometrical relaxation energy from excited state to ground state is defined as $\lambda_{rel} = \Sigma \hbar \omega_i S_i$, which can be partitioned into the

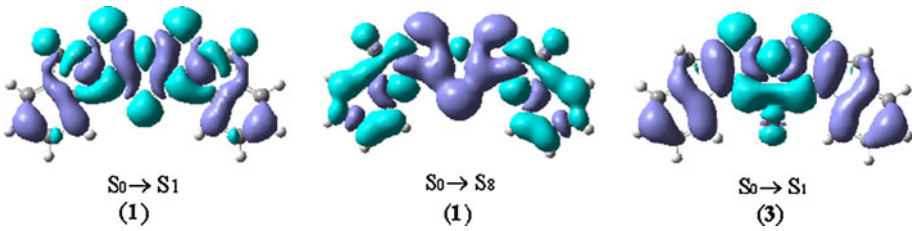

Fig. 4 Changes of electron density distribution upon the $S_0 \rightarrow S_1$ and $S_0 \rightarrow S_8$ electronic transitions of **1** and the S0 → S1 electronic transition of **3**. *Violet* and *turquoise* colors correspond to a decrease and increase in electron density, respectively

Table 2 The calculated emission energies (nm), oscillator strengths (*f*), major contributions, and experimental data of all compounds

Compounds	$\lambda_{cal.}$	*f*	Major contribution	$\lambda_{exp.}$ [a]
1	372	0.50	LUMO → HOMO (98%)	373
2	376	0.66	LUMO → HOMO (98%)	376
3	522	0.43	LUMO → HOMO (99%)	
4	534	0.51	LUMO → HOMO (99%)	524

[a] Data from reference [20]

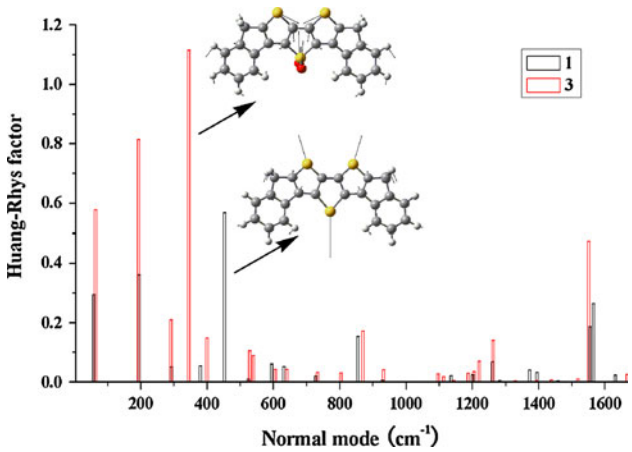

Fig. 5 Huang–Rhys factors versus the normal-mode wave numbers for **1** (*black frame*) and **3** (*red frame*). The vibration modes of their respective maximums are inserted

contribution from each normal mode. Figure 5 shows the Huang–Rhys factors versus the normal-mode wave numbers for **1** and **3** along with the vibration modes of their respective maxima. It is found that the larger Huang–Rhys factors mainly appear in low-frequency area (<500 cm^{-1}) for both **1** and **3**, which indicates that the low-frequency vibration modes may have stronger electron–phonon coupling strength during the process of electron transition. Specifically, the Huang–Rhys factors of **3** in low-frequency region are also larger than **1,** and the largest one is 1.12, which is double that of **1**. Analysis of vibration modes shows that the vibrations in low-frequency area with larger Huang–Rhys factors for **1** are the extensional vibrations of benzene rings along the long axis of molecule relative to center and the stretching vibrations of three sulfur atoms in central fused thiophenes described in Fig. 5, while for **3**, the vibrations in low-frequency region mainly originate from the vibrations of the two oxygen atoms except for the vibrations of **1** mentioned above. The geometrical relaxation energies of **1** and **3** are 1,616 and 2,310 cm^{-1}, respectively. It suggests that **1** may have stronger rigidity than **3,** and thus, the radiationless decay rate of **1** may be smaller than that of **3**. Second, the intersystem crossing to the triplet excited states as a single molecule non-radiative path was also considered by qualitatively describing the intersystem crossing rate as function of S_1-T_n energy gap [50]. The calculated excitation energy levels of **1** and **3** at their respective S_0 optimized geometries are drawn in Fig. S3. According to the energy-gap law, $S_1 \rightarrow T_n$ intersystem crossing of the dioxide **3** may be more efficient than that of **1** due to much smaller energy gap of $S_1 \rightarrow T_2$ (0.02 eV) of **3** than that of $S_1 \rightarrow T_4$ (0.25 eV) of **1**. As a result, combining with their calculated natural radiative decay rates, **1** was inferred to have larger fluorescence quantum yield than **3** in theory. As mentioned above, **3** has been proved to being a good approximation to **4**, so **4** should have smaller fluorescence quantum yield than **1** in theory, that is, the larger fluorescence quantum yield of **4** (0.72 for **4** vs. 0.01 for **1**) could not be ascribed to the introduction of thienyl-*S*,*S*-dioxide substituent at the single molecule level. Here, further argument to rationalize this abnormality was carried out as follows.

First, we excluded the influence of the alkyl chains on the fluorescence quantum yield. We replaced the hydrogen atoms in cyclopentadienes of **3** by methyl groups and then estimated its relaxation property of the excited state at the same theoretical level. The results shown in Fig. S4 reveal that the Huang–Rhys factors of the new model molecule (**3a)** in low-frequency region are also larger than that of **1** and the vibrations of methyl groups become the main contributions to the electron–phonon couplings. The geometrical relaxation energy between excited state and ground state is about 2,340 cm^{-1}, which is slightly larger than that of **3**. Therefore, the alkyl chains are expected to further deteriorate the fluorescence quantum yield at the single molecule level.

After the fluorescence quantum yield at the single molecule level was considered, the aggregate such as H-aggregation, which may induce fluorescent quenching, was finally invoked to explain the very small fluorescence quantum yield of **1**. Considering the poor solubility of **1** in chloroform solvent, which may result in large aggregated molecules, the absorption property of the dimer of **1** at optimized geometry by B3LYP-D functional was also calculated, and the comparisons of absorption spectra of single molecule, dimer and experimental one are depicted in Fig. S5. It can be found that the agreement between the simulated spectrum of dimer and the measured one of **1** is better. So we infer that there may be a great amount of absorption transitions of aggregated molecules, which may induce energy transfer or electron transfer phenomena, and these behaviors would quench efficiently the fluorescence. More importantly, the incorporation of thienyl-*S*,*S*-dioxide unit and the long solubilizing alkyl chains may expand intermolecular distances and prevent effective fluorescent quenching [15].

3.4 Transport property

In general, materials present high mobility if they have the ordered packing, especially for fused thiophenes. In contrast, the mobility of **1** was reported as low as 10^{-4} $cm^2/V{\cdot}s$. Thus, the insight into transport properties of all compounds is demanded. Consequently, the reorganization energies of all compounds investigated here were first evaluated from adiabatic potential-energy surfaces method [51, 52]. Recently, Sancho-García and Pérez-Jiménez have reported that the DFT estimate of the reorganization energy strongly depends on the ratio between the HF-like and density functional exchange, and BλLYP (%HF = 25.33) functional leads to better values [53–55]. Here, a GGA functional BPW91 and three hybrid GGA functionals, namely BPW91, B3LYP, B3PW91, and BλLYP, were employed to calculate the hole and electron reorganization energies of **1**. The results presented in Fig. S6 show that these four functionals give essentially same trend for the reorganization energy, and three hybrid functionals provide similar values. Given that not affecting the relative values of the mobilities, we still employed B3PW91/6-31G(d,p) to evaluate reorganization energies of all compounds (described in Fig. S7). Figure S7 shows that four hexyl chains have little influence on both hole and electron internal reorganization energies, while the electron reorganization energies of **3** and **4** show a large increase in comparison with **1** and **2**, because of the incorporation of thienyl-*S*,*S*-dioxide unit.

From crystal structure of **1** represented in Fig. 6a, we selected main hopping pathways and calculated their corresponding transfer integrals based on site-energy corrected method using PW91PW91 functional. Since molecules

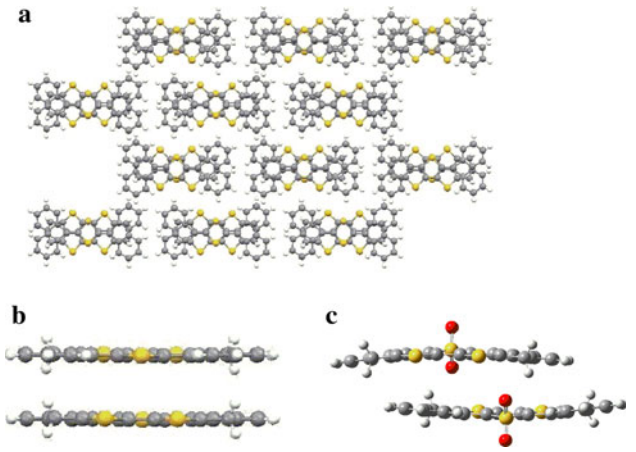

Fig. 6 **a** Crystal of **1**; **b** Major charge hopping pathway of **1**; **c** Optimized dimer of **3** based on B3LYP-D/cc-pVDZ level in OCAR 2.8.0 package

form one-dimensional π–π stack, only two major transport pathways assigned to a typical dimer were found, illustrated as Fig. 6b. The corresponding hole transfer integral and electron transfer integral are 62.5 and 20.6 meV, respectively. Inserting the values of λ and t into Marcus formula, the hole and electron hoping rates of **1** are obtained, which are 1.37×10^{13} s^{-1} and 1.82×10^{12} s^{-1}, respectively. For **3**, the stablest dimer from the result of MD simulation has been optimized (depicted in Fig. 6c) employing B3LYP-D/cc-pVDZ level in ORCA package. Its hole and electron transfer integrals calculated are 59.0 and 51.9 meV, respectively. Combining with reorganization energies, the hole hopping rate of 1.09×10^{13} s^{-1} and electron hopping rate of 1.64×10^{12} s^{-1} were obtained. Thus, **1** and **3** may have similar charge (both hole and electron) transport performances, although the electron reorganization energy of **3** is larger than that of **1**, which is ascribed to the stronger intermolecular orbital coupling of **3**. Moreover, in view of the lower LUMO energy level together with high electron hopping rate, we infer that **3** may be a good ambipolar transport material.

The hole and electron mobilities of **1** were estimated according to the values of reorganization energies and transfer integrals in the framework of Marcus theory. The calculated electron and hole mobilities are 0.02 and 0.12 $cm^2/V{\cdot}s$, respectively. The latter is sharply different from the experimental value of hole mobility, about 10^{-4} $cm^2/V{\cdot}s$ using standard semiconductor model. The difference between the theoretical and experimental values could be attributed to two aspects. One is experimental conditions, such as the polycrystalline nature of the evaporated film as the statement of experimentalists [20], the other is the large thermal fluctuation along one-dimensional transport, which may be prone to the incorporation of defects and thus induce lower carrier mobility [56].

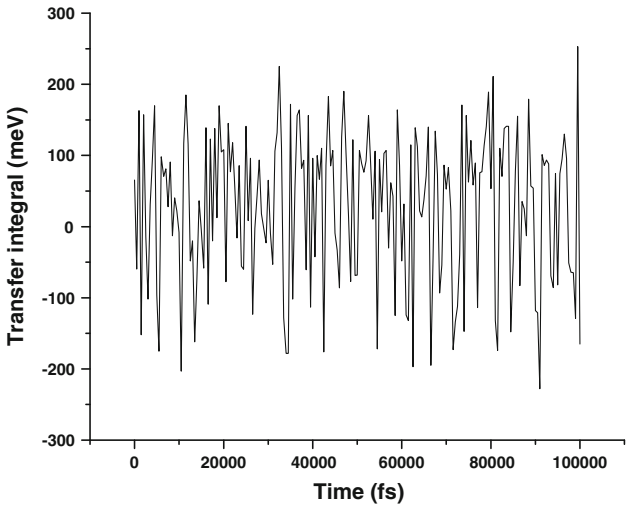

Fig. 7 Thermal fluctuation of the transfer integral (the face to face packing dimer) of **1** at 300 K

To obtain a deeper comprehension of charge transport along π–π stack, the classical MD simulation with fixed lattice constants based on supercell ($4 \times 3 \times 3$) of the crystal unit cell of **1** was carried out with COMPASS force field within the Material Studio package. Dynamic trajectories were extracted every 500 fs with a total 200 snapshots, and the transfer integral of the major dimer at each snapshot was calculated to estimate the strength of the nonlocal source of electron–phonon interaction. The thermal fluctuation of the transfer integrals, depicted in Fig. 7, is very large. It indicates that the contribution of the nonlocal interactions is so intense as to result in obvious vibration-modulated contribution to the charge transport. This significant fluctuation was considered to arise from the strong π–π intermolecular interaction along the stack direction with close distance, and there are no strong interactions in other directions. As Shuai et al. [39] mentioned, large fluctuation of the transfer integral may induce less charge-transfer rates between parts of the molecular dimers than those at the equilibrium geometry and thus induce bottleneck effect for charge transport in one-dimensional stacked chain. Here, it is concluded that the mobility of **1** would be reduced by the large disorder effect in the π–π stacked direction.

4 Conclusion

Four diindenodithienothiophene derivative materials were studied based on quantum chemical calculation in this work. Their photoluminescence and charge transport properties were discussed, especially for the influence of the incorporation of thienyl-*S*,*S*-dioxide unit on the optoelectronic properties of dithienothiophenes. The results show that thienyl-*S*,*S*-dioxide unit lowers the LUMO energy levels through facilitating the formation of bonding orbital of carbon–sulfur bond without affecting obviously HOMO energy levels, which thus makes their spectra (both absorption and emission) red-shift compared with **1** and **2**. Larger radiative decay rate and smaller radiationless decay rate of **1** than those of **3** suggest that **1** may have larger fluorescence quantum yield than **3** at the single molecular level, and finally, the aggregation performance of **1** was inferred to induce lower fluorescence quantum yield. The transport properties discussed in theory indicate that **1** may present large intrinsic hole mobility and **3** may be a good ambipolar transport material. The lower experimental value of **1** was ascribed to experimental conditions and large thermal fluctuation along one-dimensional transport.

Acknowledgments The authors gratefully acknowledge the financial support from the National Natural Science Foundation of China (Project Nos. 20703008 and 20903020), Program for Changjiang Scholars and Innovative Research Team in University (IRT0714), National Basic Research Program of China (973 Program—2009CB623605). And we also heartily thank Patrik Callis (MSU) for supplying the Bozesuite program and the state key laboratory of theoretical and computational chemistry of Jilin University for providing the computational supports.

References

1. Gigli G, Barbarella G, Favaretto L, Cacialli F, Cingolani R (1999) Appl Phys Lett 75:439. doi:10.1063/1.124403
2. Mariano F, Mazzeo M, Duan Y, Barbarella G, Favaretto L, Carallo S, Cingolani R, Gigli G (2009) Appl Phys Lett 94:063510. doi:10.1063/1.3072798
3. Horowitz G, Garnier F, Yassar A, Hajlaoui R, Kouki F (1996) Adv Mater 8:52. doi:10.1002/adma.19960080109
4. Garnier F, Horowitz G, Fichou D, Yassar A (1996) Synth Met 81:163. doi:10.1016/S0379-6779(96)03761-7
5. Ortiz RP, Casado J, Hernández V, Navarrete JTL, Letizia JA, Ratner MA, Facchetti A, Marks TJ (2009) Chem-Eur J 15:5023. doi:10.1002/chem.200802424
6. Winder C, Muhlbacher D, Neugebauer H, Sariciftci NS, Brabec C, Janssen RAJ, Hummelen JK (2002) Mol Cryst Liq Cryst 385:213. doi:10.1080/10587250290113114
7. Liu Y, Yu G, Liu YQ (2010) Sci China Chem 53:779. doi:10.1007/s11426-010-0130-z
8. Mishra A, Ma C-Q, Bauerle P (2009) Chem Rev 109:1141. doi:10.1021/cr8004229
9. Oelkrug D, Tompert A, Gierschner J, Egelhaaf H-J, Hanack M, Hohloch M, Steinhuber E (1998) J Phys Chem B 102:1902. doi:10.1021/jp973225d
10. Oelkrug D, Egelhaaf HJ, Gierschner J, Tompert A (1996) Synth Met 76:249. doi:10.1016/0379-6779(95)03464-1
11. Barbarella G, Favaretto L, Zambianchi M, Pudova O, Arbizzani C, Bongini A, Mastragostino M (1998) Adv Mater 10:551. doi:10.1002/(SICI)1521-4095(199805)10:7<551:AID-ADMA551>3.0.CO;2-Y
12. Arbizzani C, Barbarella G, Bongini A, Favaretto L, Mastragostino M, Ostoja P, Pudova O, Zambianchi M (1998) Opt Mater 9:43. doi:10.1016/S0925-3467(97)00064-5

13. Barbarella G, Pudova O, Arbizzani C, Mastragostino M, Bongini A (1998) J Org Chem 63:1742. doi:10.1021/jo972108b
14. Barbarella G, Favaretto L, Sotgiu G, Antolini L, Gigli G, Cingolani R, Bongini A (2001) Chem Mater 13:4112. doi:10.1021/cm010436t
15. Tedesco E, Della Sala F, Favaretto L, Barbarella G, Albesa-Jove D, Pisignano D, Gigli G, Cingolani R, Harris KDM (2003) J Am Chem Soc 125:12277. doi:10.1021/ja035570o
16. Suzuki Y, Okamoto T, Wakamiya A, Yamaguchi S (2008) Org Lett 10:3393. doi:10.1021/ol801136k
17. Amir E, Rozen S (2005) Angew Chem Int Ed 44:7374. doi:10.1002/anie.200501681
18. Moss KC, Bourdakos KN, Bhalla V, Kamtekar KT, Bryce MR, Fox MA, Vaughan HL, Dias FB, Monkman AP (2010) J Org Chem 75:6771. doi:10.1021/jo100898a
19. Tanaka K, Wang S, Yamabe T (1989) Synth Met 30:57. doi:10.1016/0379-6779(89)90641-3
20. Afonina I, Skabara PJ, Vilela F, Kanibolotsky AL, Forgie JC, Bansal AK, Turnbull GA, Samuel IDW, Labram JG, Anthopoulos TD, Coles SJ, Hursthouse MB (2010) J Mater Chem 20:1112. doi:10.1039/b919574b
21. Izawa T, Miyazaki E, Takimiya K (2008) Adv Mater 20:3388. doi:10.1002/adma.200800799
22. Izawa T, Miyazaki E, Takimiya K (2009) Chem Mater 21:903. doi:10.1021/cm8030126
23. Yu G, Yin SW, Liu YQ, Chen JS, Xu XJ, Sun XB, Ma DG, Zhan XW, Peng Q, Shuai ZG, Tang BZ, Zhu DB, Fang WH, Luo Y (2005) J Am Chem Soc 127:6335. doi:10.1021/ja044628b
24. Liu Y, Wang Y, Wu WP, Liu YQ, Xi HX, Wang LM, Qiu WF, Lu K, Du CY, Yu G (2009) Adv Fucnt Mater 19:772. doi:10.1002/adfm.200800829
25. Liu Y, Di CA, Du CY, Liu YQ, Lu K, Qiu WF, Yu G (2010) Chem-Eur J 16:2231. doi:10.1002/chem.200902755
26. Piacenza M, Della Sala F, Fabiano E, Maiolo T, Gigli G (2008) J Comput Chem 29:451. doi:10.1002/jcc.20804
27. Tomasi J, Mennucci B, Cammi R (2005) Chem Rev 105:2999. doi:10.1021/cr9904009
28. Frisch MJ, Trucks GW, Schlegel HB, Scuseria GE, Robb MA, Cheeseman JR, Scalmani G, Barone V, Mennucci B, Petersson GA, Nakatsuji H, Caricato M, Li X, Hratchian HP, Izmaylov AF, Bloino J, Zheng G, Sonnenberg JL, Hada M, Ehara M, Toyota K, Fukuda R, Hasegawa J, Ishida M, Nakajima T, Honda Y, Kitao O, Nakai H, Vreven T, Montgomery JA, Jr., Peralta JE, Ogliaro F, Bearpark M, Heyd JJ, Brothers E, Kudin KN, Staroverov VN, Kobayashi R, Normand J, Raghavachari K, Rendell A, Burant JC, Iyengar SS, J. Tomasi, Cossi M, Rega N, Millam JM, Klene M, Knox JE, Cross JB, Bakken V, Adamo C, Jaramillo J, Gomperts R, Stratmann RE, Yazyev O, Austin AJ, Cammi R, Pomelli C, Ochterski JW, Martin RL, Morokuma K, Zakrzewski VG, Voth GA, Salvador P, Dannenberg JJ, Dapprich S, Daniels AD, Farkas O, Foresman JB, Ortiz JV, Cioslowski J, Fox DJ (2009) Gaussian 09, Revision A.01; Gaussian, Inc., Wallingford CT
29. Cheng YC, Silbey RJ, da Silva DA, Calbert JP, Cornil J, Bredas JL (2003) J Chem Phys 118:3764. doi:10.1063/1.1539090
30. Marcus RA (1993) Rev Mod Phys 65:599. doi:10.1103/RevModPhys.65.599
31. Bredas JL, Calbert JP, Da Silva Filho DA, Cornil J (2002) Proc Natl Acad Sci U S A 99:5804. doi:10.1073/pnas.092143399
32. Valeev EF, Coropceanu V, da Silva DA, Salman S, Bredas JL (2006) J Am Chem Soc 128:9882. doi:10.1021/ja061827h
33. Yang XD, Li QK, Shuai ZG (2007) Nanotechnology 18:424029. doi:10.1088/0957-4484/18/42/424029
34. Delgado MCR, Kim EG, da Silva DA, Bredas JL (2010) J Am Chem Soc 132:3375. doi:10.1021/ja908173x
35. McMahon DP, Troisi A (2010) J Phys Chem Lett 1:941. doi:10.1021/jz1001049
36. Norton JE, Bredas JL (2008) J Am Chem Soc 130:12377. doi:10.1021/ja8017797
37. Sun H (1998) J Phys Chem B 102:7338. doi:10.1021/jp980939v
38. Martinelli NG, Olivier Y, Athanasopoulos S, Delgado MCR, Pigg KR, da Silva DA, Sanchez-Carrera RS, Venuti E, Della Valle RG, Bredas JL, Beljonne D, Cornil J (2009) ChemPhysChem 10:2265. doi:10.1002/cphc.200900298
39. Wang LJ, Li QK, Shuai ZG, Chen LP, Shi Q (2010) Phys Chem Chem Phys 12:3309. doi:10.1039/b913183c
40. Neese F, (ORCA 2.8.0, University of Bonn, Bonn, Germany, http://www.thch.uni-bonn.de/tc/orca)
41. Sancho-Garcia JC, Perez-Jimenez AJ, Olivier Y, Cornil J (2010) Phys Chem Chem Phys 12:9381. doi:10.1039/B925652K
42. Geng Y, Wang JP, Wu SX, Li HB, Yu F, Yang GC, Gao HZ, Su ZM (2011) J Mater Chem 21:134. doi:10.1039/c0jm02119a
43. Dapprich S, Frenking G (1995) J Phys Chem 99:9352. doi:10.1021/j100023a009
44. Lin BC, Cheng CP, You Z-Q, Hsu C-P (2004) J Am Chem Soc 127:66. doi:10.1021/ja045087t
45. Parac M, Grimme S (2003) Chem Phys 292:11. doi:10.1016/S0301-0104(03)00250-7
46. Gao T, Shi LL, Li HB, Zhao SS, Li H, Sun SL, Su ZM, Lu YH (2009) Phys Chem Chem Phys 11:5124. doi:10.1039/B812492B
47. Gao T, Sun S-L, Shi L-L, Li H, Li H-Z, Su Z-M, Lu Y-H (2009) J Chem Phys 130:184104. doi:10.1063/1.3126773
48. Sanchez-Carrera RS, Delgado MCR, Ferron CC, Osuna RM, Hernandez V, Navarrete JTL, Aspuru-Guzik A (2010) Org Electron 11:1701. doi:10.1016/j.orgel.2010.07.001
49. Peng Q, Yi YP, Shuai ZG, Shao JS (2007) J Am Chem Soc 129:9333. doi:10.1021/ja067946e
50. Oliva MM, Casado J, Navarrete JTL, Patchkovskii S, Goodson T, Harpham MR, Seixas de Melo JS, Amir E, Rozen S (2010) J Am Chem Soc 132:6231. doi:10.1021/ja101015q
51. Wu J, Wu S, Geng Y, Yang G, Muhammad S, Jin J, Liao Y, Su Z (2010) Theor Chem Acc 127:419. doi:10.1007/s00214-010-0730-x
52. Yang G, Si Y, Geng Y, Yu F, Wu Q, Su Z (2011) Theor Chem Acc 128:257. doi:10.1007/s00214-010-0841-4
53. Sancho-Garcia JC, Perez-Jimenez AJ (2008) J Chem Phys 129:024103. doi:10.1063/1.2951991
54. Sancho-Garcia JC (2007) Chem Phys 331:321. doi:10.1016/j.chemphys.2006.11.002
55. Sancho-Garcia JC, Perez-Jimenez AJ (2008) J Phys Chem A 112:10325. doi:10.1021/jp802160b
56. Vehoff T, Baumeier B, Troisi A, Andrienko D (2010) J Am Chem Soc 132:11702. doi:10.1021/ja104380c